Electrical Power and Energy Systems 157 (2024) 109851

Contents lists available at ScienceDirect

International Journal of Electrical Power and Energy Systems

journal homepage: www.elsevier.com/locate/ijepes

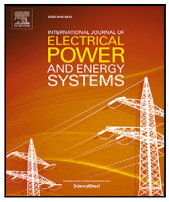

Analysis of optimal grid-forming converter penetration in AC connected offshore wind farms

Callum Henderson *, Agusti Egea-Alvarez, Lie Xu

University of Strathclyde, EEE Department, 16 Richmond St., Glasgow, G1 1XQ, City of Glasgow, Scotland

ARTICLE INFO

Keywords:
Impedance based stability
Power system stability
Converter dominated networks
Grid-forming converters
System strength

ABSTRACT

The modern electricity network is seeing a trend in the replacement of fossil fuel power plants with converter interfaced generation as worldwide efforts are made to combat climate change. New converter control structures such as grid-forming are seen as a key building block for maintaining the stability of the future power system. Moreover, wind power is the fastest growing renewable technology in the UK with ambitious targets set for installed capacity in the coming decade. While the benefits and drawbacks of the technology have been explored, little attention has been given to how many grid-forming converters will be needed to stabilise the modern network. Is there such a thing as too much grid-forming? This paper utilises an impedance-based windfarm model with the capability to include unique control systems on each turbine to present a small-signal based methodology for determining the penetration limits of grid-forming technology. Key stability and screening metrics are applied to identify the penetration that provides the strongest and most stable system. Three key points are specified: the critical, optimal and maximum penetrations. Moreover, findings suggest providing enhanced system strength via converters is only applicable to a certain extent where further interactions cause increased stability issues.

1. Introduction

The way in which power networks are operated and studied is fundamentally changing as the world strives to become carbon neutral [1]. Traditional power stations are being replaced with renewable energy systems (RES) at an ever increasing rate leading to concerns over the stability of the modern power system [2]. The loss of useful behaviour such as inertia and frequency support, system strength and fault current have all been tipped to cause significant problems if not addressed accordingly [3]. One course of remedial action is to deploy a new family of converter control topology known as grid-forming converters (GFM). The control structures aim to replicate the useful behaviour of synchronous generators (SGs) being lost from the system [4].

The largest and fastest growing RES is wind energy with the UK boasting a combined on and offshore capacity of 28.5 GW in Q3 2022 with significant expansion planned to achieve 50 GW of offshore wind by 2030 [5]. With a significant proportion of wind turbines offering an inverter-based network interface, it is clear that wind farms could play a significant role in the deployment of GFM. Furthermore, offshore windfarms are becoming increasingly connected via weak networks due to long transmission distances. Grid-following converters (GFL) have been shown to further weaken the system [6] and therefore, GFM technology has been suggested as a solution to the problems observed. Real world testing has already been completed at the Dersalloch wind farm in Scotland where the park ran in a GFM mode for several months during which a number of successful responses to unscheduled frequency and voltage events were recorded due to tripping components on the system [7]. While an important milestone for GFM wind farms, further study is required to determine the optimal number of grid-forming turbines within the farm to provide enhanced system stability.

Research on the penetration of RES and the effects on power system stability has seen significant attention in literature [8–10]. However, these approaches are more generalised looking at overall converter penetration rather than giving focus to the balance between control structures in an already converter dominated network. The limits in [8] were found based on balancing GFL converters with SGs but no consideration was given to the balance between GFL and GFM. When trying to select an approach for determining the penetration, inertia and frequency response will struggle to be the deciding factor as a 'more is better' approach tends to provide the best results regarding frequency stability. What is more likely is that the penetration of GFM technology is governed by voltage and/or harmonic stability which can be analysed by studying the impedances on the network including the converter control action.

* Corresponding author.
E-mail address: callum.henderson.9697@gmail.com (C. Henderson).

https://doi.org/10.1016/j.ijepes.2024.109851
Received 25 August 2023; Received in revised form 10 January 2024; Accepted 4 February 2024
Available online 9 February 2024

It has been reported that GFM may experience problems with synchronisation when multiple converters are connected electrically close due to poor operation of the power synchronising loop when the impedance between sources is low [11]. Moreover, GFM can be viewed as stiff voltage sources and when too many are parallelled, they begin to fight over the control of the voltage at the PCC. Hence, a theoretical maximum penetration could exist as adding more GFM lowers the overall impedance [6] causing adverse system interactions [11]. Furthermore, there are situations where a lack of GFM technology is harming system stability [12] which could provide the mechanisms behind a minimum GFM penetration. Most cases involve weak networks where the impedances are large. This leads to numerous issues such as reduced power flow, increased voltage fluctuation and poor performance of synchronisation algorithms such as phase-locked loops (PLL) used in traditional GFL control structures [13,14]. While some work has been completed trying to improve operation of PLL based algorithms [15], GFM structures have been shown to offer favourable characteristics over GFL in weak networks [6]. Moreover, when a combination of GFM and GFL is used the GFLs see significant improvement due to the presence of the GFM which provide system strength and lower the apparent impedance seen between the GFL and a stiff voltage source [6].

Selecting an appropriate technique to analyse the system that covers all interactions is challenging. Work has been completed previously looking at impedance-based stability of wind farms however, in most work the individual turbines are lumped together through some aggregation technique [16]. This has been a viable approach in the past, but it prevents individual turbines being represented and makes it more challenging to easily alter the penetration of GFM. Moreover, most approaches utilise black-box techniques as accurate converter descriptions are not readily shared by developers due to intellectual property (IP) concerns. However, these approaches become extremely challenging to apply in complex networks with hidden unstable poles and zeros appearing. More recent techniques looking at system strength including converter control action across a range of frequencies may be of aid in this regard as they offer a black-box approach without falling victim to hidden information.

This paper addresses these concerns and presents a small-signal analysis of an offshore wind farm operating both GFL and GFM turbines with the goal of determining an optimal balance between the converter technologies within the farm. The novel contributions of this work are as follows:

1. A new methodology is presented based on small-signal analysis to ascertain the GFM penetration limits within a wind park.
2. Three key grid-forming penetrations are defined: critical, optimal and maximum penetration.
3. The system strength of a wind park is analysed utilising GSIM including converter control action across a range of frequencies
4. Impedance-based stability is conducted utilising the full closed-loop transfer function of the wind park avoiding issues pertaining to open loop right-half plane poles and zeros.
5. The analysis represents each turbine individually with either GFL or GFM offering improvement over previous lumped methods where only converter penetration as a whole is analysed.

2. Analysis techniques

To determine the impact of GFM penetration on wind farm operation, two analysis methods are utilised. One based around conventional impedance-based stability updated to allow for multi-converter MIMO systems [17] and utilises disk margins to determine system robustness [18]. The second is a method for calculating system strength in converter dominated systems known as the grid-strength impedance metric (GSIM) [6].

Disk margins are selected to show system stability as they offer a significant improvement in determining system robustness over traditional gain and phase margins. Since the impedance matrices formed are MIMO systems, the SISO gain and phase margins do not accurately determine how close the analysed system is to instability, they often offer much larger margins that are actually obtainable within the real system. The disk margins consider both gain and phase perturbations in multiple channels simultaneously to give a better idea of system robustness under more realistic disturbances. In doing so, the margins are often much lower than the traditional SISO versions applied

The GSIM is a screening technique that aims to replace short-circuit ratio or short-circuit level in providing a simple number to determine how likely unstable interaction is to occur. While the value returned is a simple scalar value, the methodology applied includes all possible converter action in the network via the equivalent converter output impedances and provides a more realistic view of the system strength, which is strengthened by grid-forming and often weakened by grid-following converters. Similar to a low SCR, a low GSIM suggests that the system may be prone to increased voltage perturbation due to high impedances on the network which results in poor damping. The scale of GSIM has the same meaning as SCR and in passive network is equal to the SCR

2.1. Impedance-based stability

Impedance-based stability analysis has been widely applied in literature and is conducted by determining the interaction between a source and load impedance as a function of frequency [19]. The techniques have been applied to wind farms previously, usually by considering the farm as a single lumped converter. However in doing this, altering the balance between GFM and GFL can be challenging. Moreover, interactions between GFM voltage controllers may not be represented and therefore, not all system interactions may be covered.

When trying to model individual turbines, impedance techniques become challenging especially when combining multiple sources of the same type (voltage or current). Issues relating to hidden open-loop right half-plane (RHP) poles have been reported [20] and while work has been completed trying to remedy this for multi-converter systems [17], the approaches have yet to be applied to larger scale systems with more than two converters. In this work, full converter control structures are available therefore the closed-loop eigenvalue technique proposed in [17] is preferred. This technique can be used readily for multi-converter systems but has yet to be extended to wider scale systems.

Considering a wind farm connected to the electrical system via a long transmission line, the network including the long transmission line seen from the PCC is seen as the source with the wind farm representing the load, as shown in Fig. 1. The approach begins by solving for the current flowing through the point of common coupling (PCC) denoted by thick black bus in Fig. 1:

$$\begin{aligned}\mathbf{I}_{PCC,qd}(s) = {} & \mathbf{I}_{wf,qd}(s)(\mathbf{I}_2 + \mathbf{Z}_{n,qd}(s)\mathbf{Y}_{wf,qd}(s))^{-1} \\ & -\mathbf{V}_{GRID,qd}(s)\mathbf{Y}_{n,qd}(s)(\mathbf{I}_2 + \mathbf{Z}_{n,qd}(s)\mathbf{Y}_{wf,qd}(s))^{-1}\end{aligned} \tag{1}$$

where $\mathbf{I}_{PCC,qd}$ and $\mathbf{I}_{wf,qd}$ are the PCC and windfarm currents, respectively, $\mathbf{V}_{n,qd}$ is the network voltage, $\mathbf{Z}_{n,qd}$ and $\mathbf{Y}_{n,qd}$ are the network impedance and admittance, respectively looking left of the black bus, $\mathbf{Y}_{wf,qd}$ is the parallel windfarm admittance looking right of black bus and $\mathbf{I}_2$ is an identity matrix of rank 2. From (1), the equation describing the current at the PCC forms two closed loop systems, each with the same characteristic equation governed by the ratio between the source and load impedances. This equation can be solved using eigenvalue analysis to determining the stability. Furthermore disk margins can be used to determine robustness [18] where gain and phase margins are considered as a complex multiplicative factor f, of the form:

$$f \in D(\alpha,\sigma) = \left\{ \frac{1+\frac{1-\sigma}{2}\delta}{1-\frac{1-\sigma}{2}\delta} : \delta \in \mathbb{C}, |\delta| < \alpha \right\} \tag{2}$$

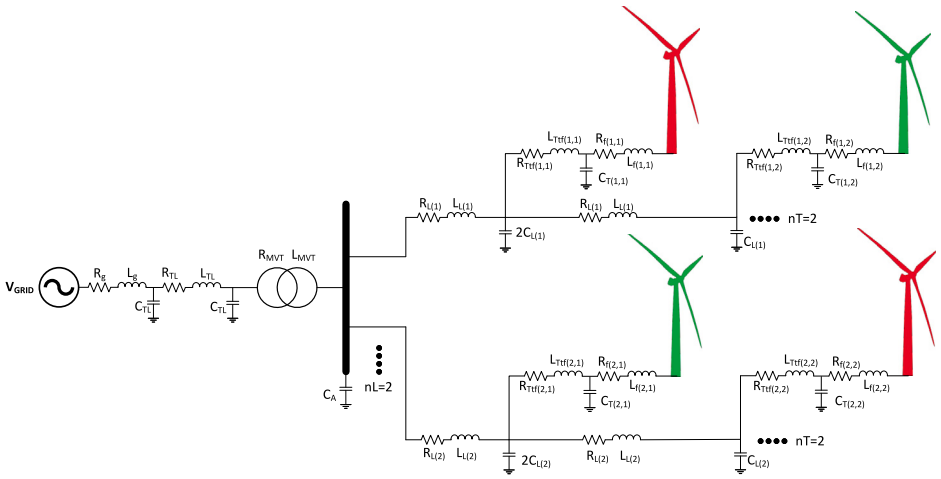

Fig. 1. Example model of programmable wind farm.

where the set $D(\alpha,\sigma)$ defines the complex set of perturbations, α is a scale parameters and if the disk skew factor σ, is selected to be 0 the overall perturbation gain can increase or decrease by the same magnitude. In this case the open-loop system is the impedance ratio:

$$L = \mathbf{Z}_{n,qd}(s)\mathbf{Y}_{wf,qd}(s) \tag{3}$$

The disk margin can then be defined as the maximum value of α that allows fL to remain stable for all $f \in D(\alpha,\sigma)$. For MIMO systems, two multiplicative factors f_1, $f_2 \in D(\alpha,\sigma)$ are applied simultaneously to both input channels for multi-loop (ML) margins.

2.2. Grid-strength impedance metric

GSIM was proposed as an alternative to SCR for determining the strength of converter dominated systems [6] however, this paper is the first application of the technique to a system containing more than two converters. The method accounts for converter action via the equivalent converter output impedance. By comparing the disk margin stability with the GSIM, conclusions can be drawn relating to how much system strength can be added with GFM before the system may become unstable due to some other interaction. The system impedance is obtained from the parallel and series combination of the impedances on the network from a specific point of view (PoV) in this case:

$$\boldsymbol{Y}_{sys}(s) = \mathbf{Y}_{n,qd}(s) + \mathbf{Y}_{wf,qd}(s) \tag{4}$$

This admittance is compared to a frequency dependent base impedance similar to the traditional application of SCR. In this case, the analysis is concerned with the balance of converters within the farm and therefore, a simple Thevenin equivalent base is sufficient for analysis. Both the base and system impedances are described in the synchronous reference frame forming a 2×2 MIMO description. Hence, proper analysis requires that the eigenvalues of each be obtained:

$$\lambda(\boldsymbol{Y}_{sys}(s)) = \begin{bmatrix} |\lambda(\boldsymbol{y}_{sys,q}(s))| \\ |\lambda(\boldsymbol{y}_{sys,d}(s))| \end{bmatrix} \tag{5}$$

$$\lambda(\boldsymbol{Z}_b(s)) = \begin{bmatrix} |\lambda(\boldsymbol{z}_{b,q}(s))| \\ |\lambda(\boldsymbol{z}_{b,d}(s))| \end{bmatrix} \tag{6}$$

where $\boldsymbol{Z}_b(s)$ is the frequency dependent base impedance which in this work is formed from Thevenin equivalent components presented in Section 4. $\lambda(\boldsymbol{Y}_{sys}(s))$ and $\lambda(\boldsymbol{Z}_b(s))$ are the eigenloci of the system admittance and base impedance, respectively. GSIM is then obtained via the element-wise multiplication (denoted $\odot$) of (5) and (6) which forms an impedance ratio:

$$\begin{bmatrix} GSIM_q(s) \\ GSIM_d(s) \end{bmatrix} = \lambda(\boldsymbol{Y}_{sys}(s)) \odot \lambda(\boldsymbol{Z}_b(s)) \tag{7}$$

where $GSIM_q(s)$ and $GSIM_d(s)$ are the q and d axis GSIM components, respectively. These components act in unison with interaction between axes to affect the stability of the grid. Therefore, the final GSIM definition combines these values into a single metric relating to the PCC voltage magnitude:

$$GSIM(s) = \sqrt{\frac{GSIM_q(s)^2 + GSIM_d(s)^2}{2}} \tag{8}$$

3. Modelling

3.1. Converters

Before modelling the wind farm it is critical to first obtain unique models of the converter controllers to be deployed into the wider system. This section describes each control type and following this, the method of obtaining the admittance of the converter structures is presented.

Grid-following converters are the most common control approach present on the network today. The name stems from the fact the controller synchronises with the external grid by 'following' a pre-existing voltage signal. A standard GFL structure that has been widely applied in literature is provided in Fig. 2 [13,17,21]. The main components include: PLL, current control loops, outer-loop power and voltage control as well as transformations, filters and delays. A full description including tuning recommendations can be found in [22].

One approach for grid-forming is to generate the converter angle by means of the power swing equation [4,23]. In this work, a simplified VSM approach is adopted utilising a PI controller to regulate active power. The PI controller in the VSM now represents both damping with the proportional term and inertia with the integral term [24]. The PI controller can be tuned accordingly to represent the dynamics of the power swing equation. The VSM approach used within this work is shown in Fig. 3 and a full description can be found in [22]. The structure excludes an internal current controller which is an approach gaining traction in literature [17,25,26]. This is due to the suggestion that the internal current control raises the converter output impedance, which may reduce the capabilities of the GFM converter [27]. Moreover, the work is concerned with quasi steady-state operation and not with fault-ride through. Therefore, converter current limiting is not of concern and cannot be modelled using the small-signal method defined in the following section.

From Figs. 2 and 3 the co-ordinate transform aligns the voltage with q-axis of the dq-frame via:

$$T(\theta) = \begin{bmatrix} cos(\theta) & sin(\theta) \\ -sin(\theta) & cos(\theta) \end{bmatrix} \tag{9}$$

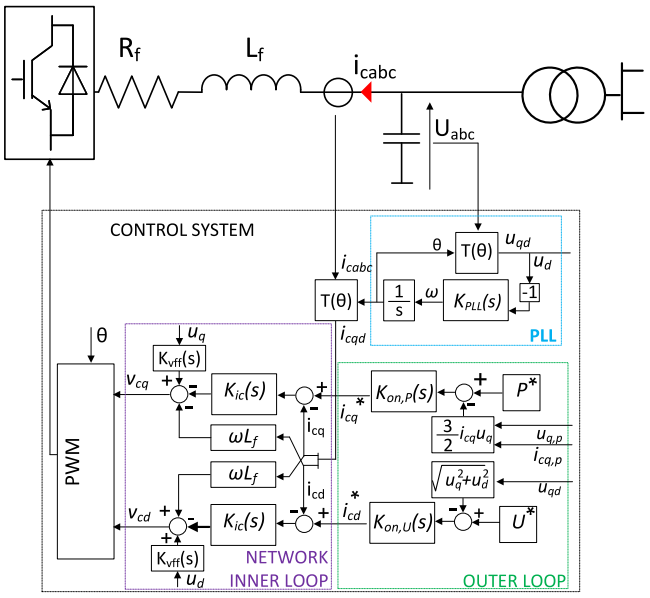

Fig. 2. GFL control diagram.

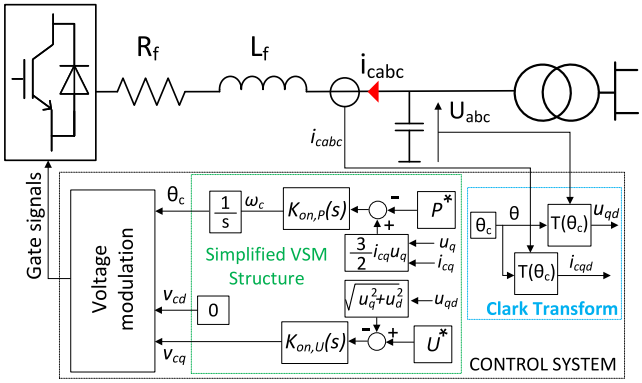

Fig. 3. VSM structure.

where θ is the angle provided from the PLL in the case of GFL or the power synchronising loop in the case of GFM.

3.2. Admittance formulation

To obtain the admittance models of the different converter controllers the structures are linearised around an operating point and expressed as state–space models. Once the model is linearised the converter admittance is classified as the ratio of the response current from the converter ($\boldsymbol{I}_c$) to the voltage disturbance at the PCC ($\boldsymbol{U}_{PCC}$):

$$\boldsymbol{Y}_c = \frac{\Delta \boldsymbol{I}_c}{\Delta \boldsymbol{U}_{PCC}} \tag{10}$$

The converter admittance is determined by the physical filter components and the control architecture. To generate the admittance from the state–space matrix the model inputs and outputs are selected to be:

$$\boldsymbol{u} = \begin{bmatrix} \Delta \boldsymbol{u}_{q,pcc} \\ \Delta \boldsymbol{u}_{d,pcc} \end{bmatrix} \tag{11}$$

$$\boldsymbol{y} = \begin{bmatrix} \Delta \boldsymbol{i}_{q,pcc} \\ \Delta \boldsymbol{i}_{d,pcc} \end{bmatrix} \tag{12}$$

The state–space then represents the converter admittance:

$$\begin{bmatrix} Y_{qq,c} & Y_{qd,c} \\ Y_{dq,c} & Y_{dd,c} \end{bmatrix} = \frac{\boldsymbol{y}}{\boldsymbol{u}} = \frac{\Delta \boldsymbol{i}}{\Delta \boldsymbol{u}} \tag{13}$$

The impedances are modelled in the synchronous reference frame to ensure all interactions can be accounted for. This process can be completed for a state–space model of any network component.

3.3. Modular wind farm

Using a modular modelling approach, a detailed small-signal impedance model can be constructed representing the wind farm with each individual turbine utilising the previous structures as inputs. This allows the fast creation of a wind park with nL lines of nT turbines. A diagram showcasing the construction of an example windpark with nL = 2 and nT = 2 is shown in Fig. 1. The red turbines indicate GFL while the green represents GFM. The ellipsis on the diagram indicate where repetition of the same model can occur up to the number of lines and turbines. Cables are modelled as PI sections with TL subscript representing the longer transmission line from the medium voltage transformer (MVT) to the high voltage transformers (HVT). The HVT is modelled as a Thevenin equivalent. Terms denoted subscript L represent the cables between turbines. Each turbine can be enabled with any of the control structures previously discussed. The turbines are connected to the line via an RLC filter and another RL component representing the turbine transformer.

The following assumptions are made to allow modelling: each turbine is equally spaced with the same line length, each turbine has a set active power operating point of either 0 or 0.5 p.u. that can be set independently for each turbine but are grouped to reduce the number of results. Moreover, the mechanical sub-systems are disregarded here. The impedance of the converter seen from the AC side is largely governed by the grid-side converter control structure, therefore the DC-link is modelled as an infinite source to reduce some computational burden. Finally, for strength and stability tests the wind park is assumed to be connected to a simplified Thevenin network with a specific SCR or GSIM. The analysis is concerned with penetration of GFM solely to stabilise the operation of the windfarm and therefore, a simplified representation of the remaining network and connection cables is sufficient [28–30]

The model can be verified using a time domain model of 2 lines of 2 turbines, Since the remaining lines and turbines in the small-signal impedance model are generated via repetition, this number of turbines is sufficient to verify the model for a larger system. The verification is completed by completing a frequency sweep of the time domain models looking in from the primary side of the medium voltage transformer. Series connected voltage sources are connected to the PCC and used to inject three-phase small magnitude disturbances (0.01–0.05 p.u.) from (1–1000 Hz) in the positive and negative sequence. The resultant combined voltage and current responses of the turbines are recorded in the abc-frame before being transformed during post-processing to dq-components. Positive and negative sequence injections are used to obtain two linearly independent operating points which are then utilised in the process described in [31] to obtain the admittance of the time domain model in the synchronous reference frame. Note that only balanced voltage conditions are considered in this work. Hence, the negative sequence injections are only used to create the second operating point needed to solve for the converter admittance under these balanced conditions The two models are compared in Fig. 4.

From Fig. 4, a good match between the impedance model and the time domain frequency sweep is observed throughout the frequency range. There are discrepancies around 1000 Hz where resonances are visible due to the instability of the time domain model in response to injections around these frequencies. However, the fact that the time domain model resonates to instability at these frequencies provides a verification in itself.

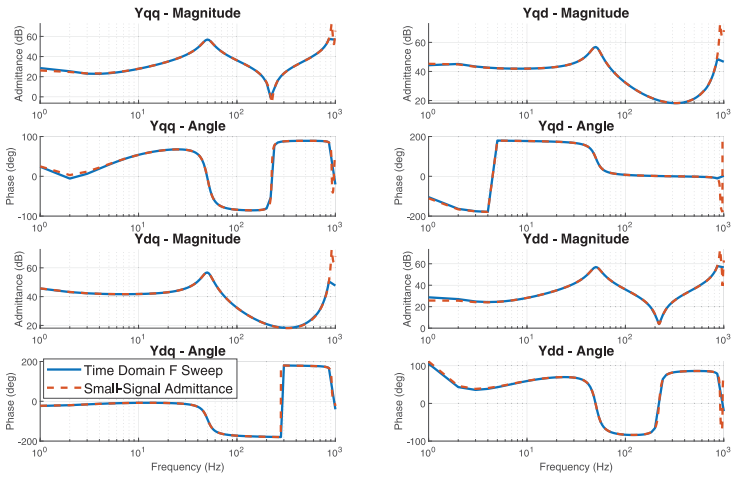

Fig. 4. Wind farm impedance validation.

Table 1
Wind farm parameters.

Parameter	Symbol	Value
Turbine voltage level	V_t	690 V
Array voltage level	V_a	66 kV
Export voltage level	V_e	220 kV
Array line resistance	R_a	0.14 Ω/km
Array line inductance	L_a	0.41 mH/km
Array line capacitance	C_a	0.19 μF/km
Export line resistance	R_e	0.047 Ω/km
Export line inductance	L_e	0.406 mH/km
Export line capacitance	C_e	0.208 μF/km

Table 2
Single line GFM investigations, Red = GFL, Green = GFM.

Topology	GSIM	DM
	0.993	0
	1.476	0.352
	1.473	0.345
	1.470	0.340
	1.467	0.338
	1.465	0.339

4. Wind farm study

The wind park was constructed with five lines of five 3 MW turbines ($nL = 5$, $nT = 5$) giving a combined power of 75 MW. This implementation is based around the CIGRE benchmark provided in [30] but utilising 3 MW turbines. Parameters for the wind farm model can be found in Table 1 with controller tuning parameters provided in Appendix Through initial testing it was determined that the position of a GFM turbine within any given line did not produce significantly different results, which can be viewed in Table 2. This was due to the significantly lower impedance of the array cables compared to the export cables.

From Table 2, the green turbine indicates a GFM controller with the red representing GFL in a line of five turbines. The position of the GFM turbine is moved along the line in each subsequent row of the table. With no GFM present the system is unstable and the strength is rated below 1. The introduction of the GFM turbine stabilises the system and the GSIM reaches almost 1.5 with no significant difference in disk margin or GSIM for the varying positions of GFM turbine on the line. Hence, the position of the turbines within the wind farm are not studied further in this work

Following this, the GFM penetration within the farm, defined as the ratio of the number of GFM turbines to the total number of turbines in the farm as a percentage, was varied by switching each individual turbine controller from GFL to GFM and recording key stability and strength data for each iteration. The park was connected to the onshore connection point via an AC transmission line with three cable lengths used: 50 km, 100 km and 150 km. Each cable was modelled as a PI section with reactive compensation split between both ends and the middle of the line. The strength and robustness is then analysed at the offshore connection point from the PoV of another system looking in. The GSIM of the onshore connection point was set to 2 (equivalent to SCR = 2) resulting in a GSIM at the offshore connection point of 1.48, 1.27 and 0.86, for the respective ascending line lengths.

The network and transmission line was represented as $\mathbf{Z}_{n,qd}(s)$ with the full farm admittance contained within $\mathbf{Y}_{wf,qd}(s)$. The farm admittance was calculated for an increasing number of integer GFM turbines from 0 to 25 and the GSIM and disk margin were calculated as in the previous subsection. The GSIM and robustness is analysed and provided in Fig. 5(a) considering all turbines at 0.5 p.u. active power for the three different lengths of export cable. The small-signal analysis conducted is used to provide an initial estimate of the strength and stability of the wind farm and is only valid for small disturbances around the operating point at which the model is linearised. This provides a good measure of how the converter will behave under standard operating conditions. However, accounting for slower acting supervisory controls such as deloading algorithms and other environmental factors such as wind availability can only be included with multiple operating points Hence, the same analysis is provided considering all turbines are at 0 p.u. active power in Fig. 5(b).

From Fig. 5(a), the strength of offshore connection point rises steadily with GFM penetration. The initial strength is significantly lower for the longer transmission lines as expected. However, when GFM penetration passes a certain threshold the strength appears to

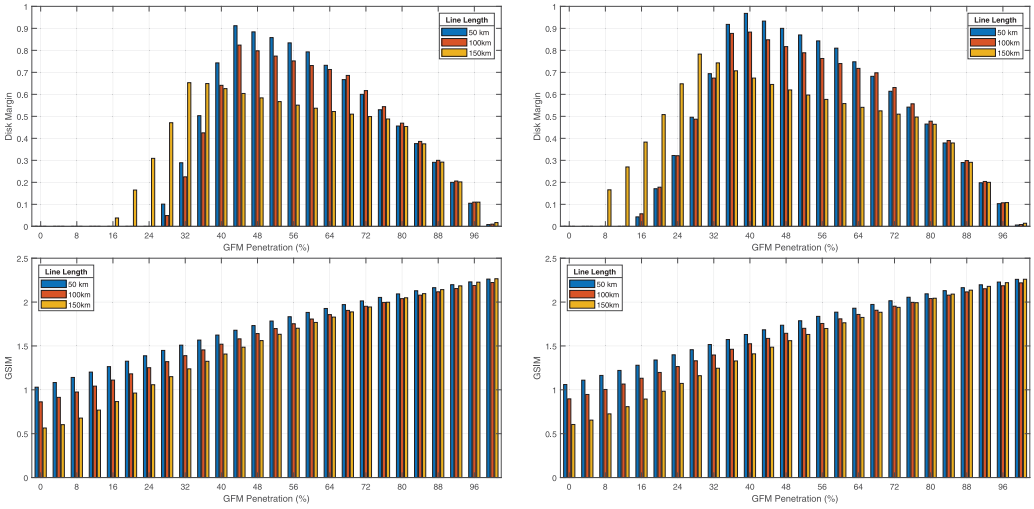

(a) 0.5 p.u. active power (b) 0 p.u. active power

Fig. 5. Disk margin and GSIM at different penetrations of GFM turbine.

not depend on the length of the line as all of the strength is being provided within the farm. This occurs when the strength of the offshore connection point exceeds that of the onshore connection point therefore negating any detrimental effects of the longer line length. However, the increased strength provided from within the windfarm results in reduced system stability, likely due to further interactions between the increased number of GFM which lowers the equivalent impedances seen between the converters

Three key penetrations are defined for each transmission line length. The critical penetration, which is minimum number of GFM turbines to stabilise the system. This is 16% for the 150 km line and 28% for the 50 km and 100 km. The longer line has a lower critical penetration than the shorter lines which appears counter intuitive but the reason for this can be explained by analysing the frequency dependent GSIM in the following pages. For now, despite less GFM being required to initially stabilise the system for a longer line, it is important to consider that the maximum achievable robustness always occurs for the shortest transmission line length.

The second key penetration is the optimal penetration of GFM converters. This is the penetration that provides the largest robustness, not the greatest strength. The optimal penetration is 32% for the 150 km line while 44% for the 50 km and 100 km lines. Beyond this penetration, the robustness of the wind farm seen from the network begins to reduce slightly with increased GFM. However, the GSIM rating of strength continues to rise. The results suggest that providing too much virtual stiffness beyond the original connection point can result in reduced stability, likely due to the increased work of the GFM converters. GFM converters do less work to strengthen the network as the system becomes stiffer as the smaller network impedance begins to dominate behaviour. Moreover, the negative effect of the GFL was exacerbated.

The final key penetration is known as the maximum penetration which is the point after which the stability of the system begins to decay rapidly. This is 80% for the 150 km line, 72% for the 100 km line and 68% for the 50 km line. The maximum penetrations appear to approximately align with the point at which the offshore GSIM is restored back to the same value provided initially at the onshore connection point excluding any action from the wind farm or cables. This is the point where the GFM turbines fully negate the weakening provided by the long export cable. Strengthening beyond this provides a significant reduction of stability up to 100% penetration. The fully GFM wind park is stable but is very close to being critically stable and should be avoided.

From Fig. 5(b), the effect of reduced operating point had a significant effect on the three key penetrations discussed. Less GFM was needed to stabilise each system with the critical penetrations dropping to 8% for the 150 km line and 16% for the 100 km and 50 km lines. The optimal penetrations fall to 28% for the 150 km line and 40% for the 100 km and 50 km lines. Conversely, the maximum penetration is increased, rising to 84%, 80% and 72% for the 150 km, 100 km and 50 km lines, respectively. The maximum penetration again appeared to coincide with the point at which the stiffness of offshore connection becomes approximately equal to the onshore connection point. Therefore, a sudden drop in wind should not be detrimental if the GFM penetration is sized for higher power levels.

As discussed, the fact that the longer transmission line offers the lowest critical penetration appears counter intuitive. In reality, this problem indicates the requirement to analyse strength at frequencies other than the fundamental. In this section, the GSIM is plotted as a function of frequency for the three transmission lines at the critical penetration for the 150 km line which was 16% in Fig. 6(a). Following this, the penetration was increased to the critical value determined for the 50 km and 100 km lines which was 28% and the resultant frequency dependent GSIM traces are plotted in Fig. 6(b).

From Fig. 6(a), it can be seen that the shorter line offers a slightly higher strength rating at the fundamental frequency which would usually indicate a more stable system. However, two large poles in GSIM can be seen for the 50 km and 100 km lines around 50 Hz in the dq-frame representing a high rate of change of strength which may indicate instability. These poles are the reason the system requires further GFM penetration to stabilise. The system with the 150 km line does not exhibit this same interaction and stabilises for a lower critical penetration.

From Fig. 6(b), the greater penetration of GFM removes the large poles that were of concern previously and results in a stable system. This suggests that the critical penetration of the shorter lines (50 km, 100 km) was related to an interaction that was not at the fundamental frequency. It was likely due to an interaction between the wind park and the transmission line which had poorly designed compensation and required more GFM to dampen the oscillation. Considering that the compensation was deliberately designed for the 150 km line, it makes sense that poor behaviour is observed for the shorter lines. Re-tuning of the controllers or properly sizing the compensation could remove this pole and may reduce the critical penetration of the shorter lines. What is clear is the requirement to analyse the system strength as a function of frequency as the fundamental frequency information is not sufficient for characterising the modern network.

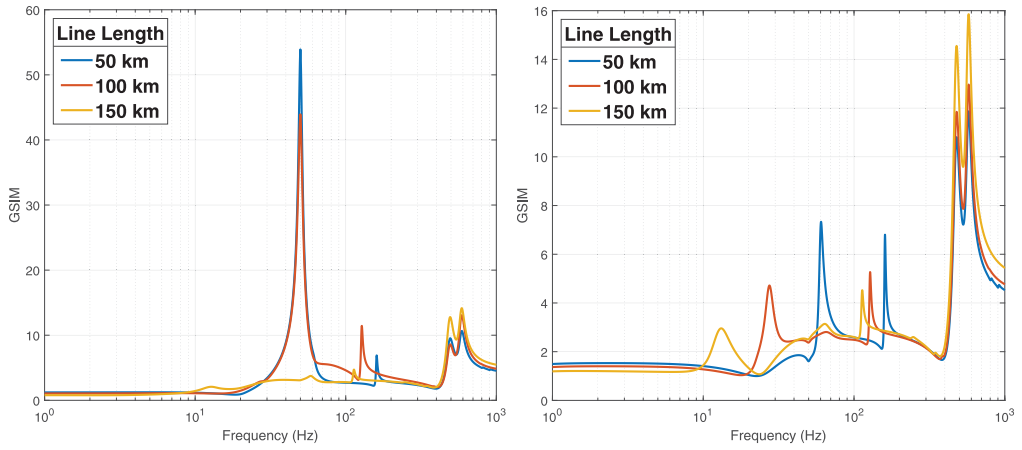

(a) 16 % penetration GFM Turbine (b) 28 % penetration GFM Turbine

Fig. 6. Frequency dependent GSIM at 0.5 p.u. active power.

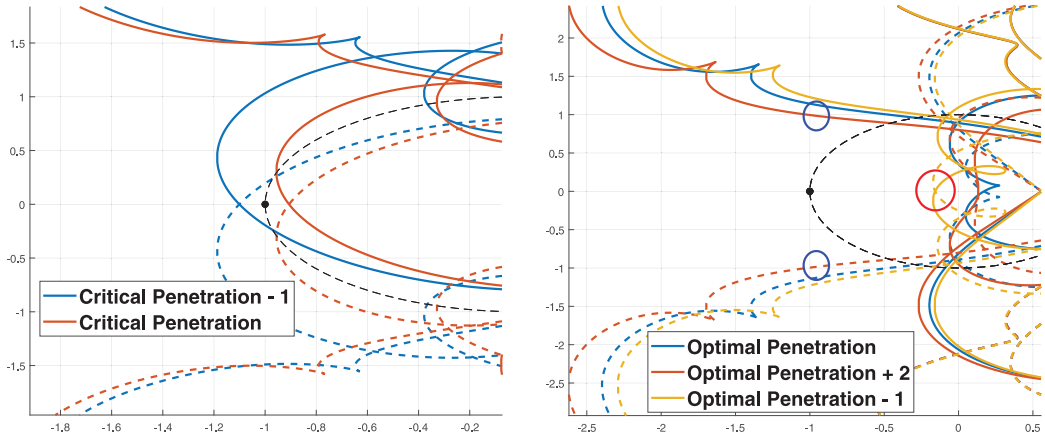

(a) Critical Penetration (b) Optimal Penetration

Fig. 7. First eigenloci with 100 km line connection.

The key penetrations can be further investigated using Nyquist contours to determine which eigenloci offers reduced stability and why. In the case of critical penetration the instability is related to the first eigenloci and a graphical representation of the stability margins at this penetration for the 100 km line is shown in Fig. 7(a). The eigenloci for the optimal penetration is then shown in Fig. 7(b).

From Fig. 7(a), the encirclement of the critical point is clearly visible when the GFM penetration is 1 turbine below the critical penetration. When another turbine is added the encirclement is removed and moves to the right of the critical point indicating stability. It should noted that the contour begins to move closer towards the critical point directly above and below the critical point as the penetration is increased. This important as it provides the mechanism for obtaining the optimal penetration.

From Fig. 7(b), the optimal penetration is shown in blue. When the penetration is below this level (shown in yellow), the contour still contains the loop that caused instability around the critical penetration (red circle). At the optimal penetration this loop is moved further away and reduces in size. At this point, the disk margin becomes related to the distance directly above and below the critical points (blue circles). As the penetration is increased beyond the critical point, this part of the contour begins to move closer to the critical point reducing the robustness of the system as the strength is further increased. This provides the mechanism for the optimal penetration as balancing these two parts of the traces becomes critical. The loop causing the instability (red circle) occurs at a lower frequency and is the reason the GSIM and disk margin have a strong correlation as penetration increases beyond critical. The loops providing the balance at the optimal penetration (blue circles) are related to higher frequencies. Therefore, as these move closer to the critical point the system strength at the fundamental frequency cannot capture this. Studying the strength across the frequency range is required to identify this point. When considering the mechanism behind the maximum penetration the problem is relates to the second eigenloci. Since the introduction of each GFM adds only a limited number of states relating to the power and voltage control loops, the reduced stability is likely due to increased interactions of these control systems between each turbine. This effect is exacerbated as the equivalent impedance and therefore damping seen between converters reduces with the introduction of further GFM As the system approaches maximum penetration the second eigenloci exhibits similarly reduced robustness as the contours begin to close towards the critical point similar to the effect observed in Fig. 7(b).

5. Conclusion

Using the proposed techniques, analysis of the strength and stability of an offshore wind farm was conducted. Three key penetration levels were identified: critical, optimal and maximum penetration. Critical penetration is the minimum number of turbines to stabilise the system where the strength is great enough to connect but the robustness remains low. The optimal penetration is the number of GFM devices

that provide the greatest system robustness, not system strength. Finally, the maximum penetration occurs when further increasing the penetration of GFM causes the stability to rapidly decay. The maximum penetration tended to coincide with when the offshore connection point was restored to the initial strength of the onshore connection point. Moreover, the GSIM provided at the fundamental frequency did not provide the full picture of system stability and considering strength as a function of frequency was required to identify problematic interactions that occurred far from the fundamental.

It is clear that GFM technology can be of benefit to offshore windfarm operation from a voltage stability standpoint. However, too much GFM can cause the converters to exhibit increased interactions due to reduced impedance between turbines. It should be noted that while installing GFM alongside energy storage is likely the most preferable option, the improvement in voltage stability presented in this work is not energy intensive and can be provided without storage. The GFM control algorithm and tuning can play a large role in determining the required penetration of GFM. Future approaches are dependent on scenario but could look to have a small number of stiff GFM converters strictly controlling voltage. However, this leaves the system at greater risk if a GFM converter is lost during faults, outages or abnormal system conditions. Conversely, a high number of weaker GFM converters could be used so as to improve parallel operation and reduce the risk from a single converter loss. Clearly a mix of converter technology is required and a number of considerations must be made

CRediT authorship contribution statement

Callum Henderson: Writing – review & editing, Writing – original draft, Validation, Methodology, Formal analysis, Data curation, Conceptualization. **Agusti Egea-Alvarez:** Writing – review & editing, Funding acquisition, Conceptualization. **Lie Xu:** Writing – review & editing, Resources, Funding acquisition, Conceptualization.

Declaration of competing interest

The authors declare the following financial interests/personal relationships which may be considered as potential competing interests: Callum Henderson reports financial support was provided by Engineering and Physical Sciences Research Council.

Data availability

Data will be made available on request.

Acknowledgements

Callum Henderson is supported by the Engineering and Physical Sciences Research Council, [EP/R513349/1]. All results can be fully reproduced using the methods and data described in this paper and references provided. All authors approved the version of the manuscript to be published.

Appendix. Controller tunings

Parameter	Symbol	Value
GFL current control P gain	$k_{I,p}$	0.0505 V/A
GFL current control I gain	$k_{I,i}$	1.587 V/A
GFL power control P gain	$k_{flP,p}$	5×10^{-4} A/W
GFL power control I gain	$k_{flP,i}$	0.1 A/W
GFL voltage control P gain	$k_{flV,p}$	6 A/V
GFL voltage control I gain	$k_{flV,i}$	20 A/V
GFL PLL P gain	$k_{pll,p}$	1.557 rad/sV
GFL PLL I gain	$k_{pll,i}$	175 rad/sV
GFM power control P gain	$k_{flP,p}$	3.19×10^{-6} rad/Ws
GFM power control I gain	$k_{flP,i}$	5.24×10^{-5} rad/Ws
GFM voltage control P gain	$k_{flV,p}$	1 A/V
GFM voltage control I gain	$k_{flV,i}$	100 A/V
GFM active power filter time constant	τ_{apf}	0.01 s
GFM PCC voltage filter time constant	τ_{pvf}	0.01 s

References

[1] Masson-Delmotte V, Zhai P, Pirani A, et al. IPCC, 2021: Summary for policymakers. Report, 2021.
[2] The Rt Hon Anne-Marie Trevelyan MP and The Rt Hon Alok Sharma KCMG MP. End to coal power brought forward to October 2024. 2021.
[3] Tielens P, Van Hertem D. Grid inertia and frequency control in power systems with high penetration of renewables. 2012.
[4] D'Arco S, Suul JA. Virtual synchronous machines; Classification of implementations and analysis of equivalence to droop controllers for microgrids. IEEE.
[5] Energy trends december 2022. Department for Business Energy & Industrial Strategy, UK Govt; 2022.
[6] Henderson C, Egea-Alvarez A, Kneuppel T, Yang G, Xu L. Grid strength impedance metric: An alternative to SCR for evaluating system strength in converter dominated systems. IEEE Trans Power Deliv 2023;1–10.
[7] Roscoe A, Knueppel T, Da Silva R, Brogan P, Gutierrez I, Elliott D, Perez Campion J-C. Response of a grid forming wind farm to system events, and the impact of external and internal damping. IET Renew Power Gener 2020;14(19):3908–17.
[8] Ierna R, Zhu J, Urdal H, Roscoe A, Yu M, Dyśko A, Booth C. Effects of VSM convertor control on penetration limits of non-synchronous generation in the GB power system. 2016.
[9] Collados-Rodriguez C, Cheah-Mane M, Prieto-Araujo E, Gomis-Bellmunt O. Stability and operation limits of power systems with high penetration of power electronics. Int J Electr Power Energy Syst 2022;138:107728.
[10] Yu M, Roscoe AJ, Dyśko A, Booth CD, Ierna R, Zhu J, Urdal H. Instantaneous penetration level limits of non-synchronous devices in the British power system. IET Renew Power Gener 2017;11(8):1211–7.
[11] Zhang L. Modeling and control of VSC-HVDC links connected to weak AC systems (Ph.D. thesis), 2010.
[12] Davari M, Mohamed YA-RI. Robust vector control of a very weak-grid-connected voltage-source converter considering the phase-locked loop dynamics. IEEE Trans Power Electron 2017;32(2):977–94.
[13] Wu G, Sun H, Zhao B, Xu S, Zhang X, Egea-Alvarez A, Wang S, Li G, Li Y, Zhou X. Low-frequency converter-driven oscillations in weak grids: Explanation and damping improvement. IEEE Trans Power Syst 2021;36(6):5944–7.
[14] Ray I, Tolbert LM. The case against phase-locked loops in weak AC grids. IEEE.
[15] NERC. Integrating inverter-based resources into low short circuit strength systems - reliability guideline. 2017.
[16] Badr MA, Atallah AM, Bayoumi MA. Comparison between aggregation techniques for PMSG wind farm. Energy Procedia 2015;74:1162–73.
[17] Henderson C, Egea-Alvarez A, Xu L. Analysis of multi-converter network impedance using MIMO stability criterion for multi-loop systems. Electr Power Syst Res 2022;211:108542.
[18] Seiler P, Packard A, Gahinet PA. An introduction to disk margins. IEEE Control Syst Mag 2020.
[19] Sun J. Impedance-based stability criterion for grid-connected inverters. IEEE Trans Power Electron 2011;26(11):3075–8.
[20] Liu F, Liu J, Zhang H, Xue D. Stability issues of Z + Z type cascade system in hybrid energy storage system (HESS). IEEE Trans Power Electron 2014;29(11):5846–59.

[21] Egea-Alvarez A, Fekriasl S, Hassan F, Gomis-Bellmunt O. Advanced vector control for voltage source converters connected to weak grids. IEEE Trans Power Syst 2015;30(6):3072–81.
[22] Henderson C, Vozikis D, Holliday D, Bian X, Egea-Àlvarez A. Assessment of grid-connected wind turbines with an inertia response by considering internal dynamics. Energies 2020;13(5).
[23] Abdelrahim AM, Mckeever P, Smailes M, Egea-Àlvarez KH. Modified grid forming converter controller with fault ride through capability without PLL or current loop.
[24] Henderson C. Interactions of grid-forming converter for windfarm applications (Ph.D. thesis), 2023.
[25] Zhong Q-C, Weiss G. Synchronverters: Inverters that mimic synchronous generators. IEEE Trans Ind Electron 2011;58(4):1259–67.
[26] Abdelrahim A, Smailes M, Ahmed KH, McKeever P, Egea-Alvarez A. New fault detection algorithm for an improved dual VSM control structure with FRT capability. IEEE Access 2021;9:125134–50.
[27] Henderson C, Egea-Alvarez A, Li R, Xu L, Da Silva R, Kinsella A, Gutierrez I, Pabat-Stroe R. Exploring an impedance-based SCR for accurate representation of grid-forming converters. 2022.
[28] Liu B, Li Z, Zhang X, Dong X, Liu X. Impedance-based analysis of control interactions in weak-grid-tied PMSG wind turbines. IEEE J Emerg Sel Top Circuits Syst 2021;11(1):90–8.
[29] Kocewiak LH, Hjerrild J, Bak CL. Wind turbine converter control interaction with complex wind farm systems. IET Renew Power Gener 2013;7(4):380–9.
[30] Kocewiak L, Blasco-Gimenez R, Buchhagen C, et al. Overview, status and outline of stability analysis in converter-based power systems. 2020.
[31] Gong H, Wang X, Yang D. DQ-Frame impedance measurement of three-phase converters using time-domain MIMO parametric identification. IEEE Trans Power Electron 2021;36(2):2131–42.